energies

MDPI

Article

Virtual Signal Injection Maximum Torque per Ampere Control Based on Inductor Identification

Ning-Zhi Jin, Hong-Chao Chen, Dong-Yang Sun *, Zhi-Qiang Wu, Kai Zhou and Long Zhang

Engineering Research Center of Automotive Electronics Drive Control and System Integration, Ministry of Education, Harbin University of Science and Technology, Harbin 150080, China; sharon0716@126.com (N.-Z.J.); hongchaochen311@163.com (H.-C.C.); zhiqiangwu1120@163.com (Z.-Q.W.); zhoukai@hrbust.edu.cn (K.Z.); longz919@163.com (L.Z.)

* Correspondence: dongyang0521@126.com

Abstract: The high-frequency signal injection-type maximum torque per ampere (MTPA) algorithm is usually employed to control the operation of interior permanent magnet synchronous motors (IPMSMs). The MTPA algorithm exhibits good dynamic performance and anti-interference ability. However, due to the injection of a high-frequency current signal, problems such as torque ripple and additional loss are encountered. Therefore, in this paper, a virtual signal injection control (VSIC) method that does not require actual injection is proposed for solving the aforementioned problems while yielding good performance. However, in the control process of the proposed method, the d-axis inductance parameter affects the accuracy of the torque information, resulting in errors in the system. To solve this problem, an online identification algorithm of model reference adaptive systems (MRAS) based on the Popov super stability theory as the basis for the design of the adaptive law is proposed in this paper. The d-axis inductance parameter of the motor is obtained in real-time and then introduced into the control system by using the VSIC method. Finally, VSIC-type MTPA control based on inductance identification is realized. The proposed algorithm does not depend on the design parameters of the motor and exhibits good dynamic response and anti-interference performance.

Keywords: permanent magnet synchronous motor; model reference adaptive system; virtual signal injection control; maximum torque per ampere

Citation: Jin, N.-Z.; Chen, H.-C.; Sun, D.-Y.; Wu, Z.-Q.; Zhou, K.; Zhang, L. Virtual Signal Injection Maximum Torque per Ampere Control Based on Inductor Identification. *Energies* **2022**, *15*, 4851. https://doi.org/10.3390/en15134851

Academic Editors: Lorand Szabo and Feng Chai

Received: 11 May 2022
Accepted: 30 June 2022
Published: 1 July 2022

1. Introduction

With the advancements in high-performance permanent magnet materials, especially the emergence of rare-earth permanent magnet materials, the performance of interior permanent magnet synchronous motors (IPMSMs) has been greatly improved [1]. Compared with the traditional electric excitation motor, the IPMSM offers the advantages of simple structure, reliable operation, small size, low weight, low loss, high efficiency, and superior performance [2]. The maximum torque per ampere (MTPA) algorithm is widely employed as an efficient control method for IPMSMs. It can output the maximum torque under a certain stator current, thereby improving the operating efficiency of the entire system [3].

The mainstream MTPA control methods include direct formula calculation, parameter identification, table look-up, automatic search, and high-frequency signal injection.

In the direct formula calculation method, the minimum value of the electromagnetic torque equation is obtained by derivation, and then the value of the stator current on the alternating and direct axis components is directly obtained [4]. Although the direct formula calculation method is relatively simple, the parameters change during the operation. The parameter identification method can obtain accurate motor parameters in real-time and improve the running accuracy of the motor by utilizing the direct formula method combined with online parameter identification. However, this method involves tedious parameter monitoring and estimation; thus, it requires the controller to have high computing power and additional hardware [5]. In view of the problems encountered in the formula calculation

method, scholars proposed the table look-up method [6]. The table look-up method simplifies the computational complexity and can take into account the parameter change factors, but it takes up a lot of storage space and requires a large offline test workload. In the automatic search method, the vector angle of the stator current is adjusted by continuously giving a small step angle under the steady-state operation of the system to achieve the optimal control strategy of MTPA [7]. The automatic search method can automatically and gradually approach the MTPA trajectory when the parameters change, but the convergence speed and torque control accuracy are low. The high-frequency signal injection method involves observing the feedback amount of the high-frequency signal injected into the system and calculating and analyzing it to obtain the optimal working state [8,9]. The high-frequency signal injection method adjusts the optimal operating point of the MTPA control in real-time according to the motor torque pulsation generated by the injected signal, but the injected high-frequency current increases the system torque pulsation and results in increased power loss. To solve this problem, a virtual signal injection control (VSIC) method is proposed. This method is basically the same as the high-frequency signal injection method. The sine wave signal is virtually injected into the stator current angle so that the torque change information of the motor is included in the motor torque model, and the torque information containing high-frequency signals is extracted to determine the degree of deviation, which definitely avoids the high-frequency pulsation caused by the actual signal injection [10,11]. However, the VSIC method is related to the inductance parameters of the motor. When the motor parameters are inaccurate, it will deviate from the optimal operating point. Therefore, introducing an appropriate parameter identification method into the VSIC system can effectively improve the operation accuracy of the control system.

Online identification has been widely used due to its good real-time performance. Online identification methods mainly include recursive least squares, extended Kalman filter, model reference adaptive system (MRAS), and neural networks.

The recursive least squares method is the most widely used online identification method in engineering. In this method, the data obtained in the previous step is corrected according to the data obtained in the current step based on the estimated value of the model parameters in the previous step to obtain the model parameters at the current step [12,13]. However, data saturation occurs during the recursive operation process, thus requiring high system hardware and software programming. The extended Kalman filter method integrates the discrete space model into the filtering algorithm and realizes the optimal estimation of the system state by making the estimated covariance reach the minimum value [14,15]. When the extended Kalman filter method identifies multiple parameters at the same time, the operation process becomes more complicated, which increases the difficulty. The core idea of the MRAS method is to gradually converge to the actual parameters in the reference model by adjusting the parameters of the adjustable model and through the pre-designed adaptation law [16]. The MRAS method is simple in principle, accurate in identification, and fast in convergence. The neural network method can obtain better convergence characteristics, but its algorithm is very complex; thus, it is subject to many limitations in practical applications [17]. With further advances in the field of parameter identification in recent years, many new identification methods have been established. A previous study proposed the identification of PMSM parameters by using the particle swarm algorithm combined with cloud model theory, which has fast convergence speed, high precision, and efficient local evolution and mutation capabilities, avoiding the problem of easily falling into the local maximum that is encountered in the traditional particle swarm algorithm [18]. A previous study employed a genetic algorithm in a Markov chain model for parameter identification, taking into account the identification speed and accuracy [19].

To sum up, in this paper, the MTPA control of the IPMSM is realized using the virtual signal injection control (VSIC) method to improve the operation efficiency of the motor. Moreover, according to the influence of d-axis inductance parameters on the accuracy of

torque information, the MRAS is proposed to identify the motor parameters online. Finally, the MRAS and MTPA are combined to form the overall control system, and the MTPA control based on real-time online identification of inductance is realized.

2. IPMSM Mathematical Model and MTPA Control

The voltage of the IPMSM in the d-q coordinate system can be expressed as follows:

$$\begin{cases} u_{\mathrm{d}} = Ri_{\mathrm{d}} - \omega L_{\mathrm{q}} i_{\mathrm{q}} + L_{\mathrm{d}} \frac{\mathrm{d}i_{\mathrm{d}}}{\mathrm{d}t} \\ u_{\mathrm{q}} = Ri_{\mathrm{q}} + \omega(\psi_{\mathrm{f}} + L_{\mathrm{d}} i_{\mathrm{d}}) + L_{\mathrm{q}} \frac{\mathrm{d}i_{\mathrm{q}}}{\mathrm{d}t} \end{cases}, \tag{1}$$

The electromagnetic torque can be expressed as follows:

$$T_{\mathrm{e}} = 1.5p(\psi_{\mathrm{f}} i_{\mathrm{q}} + (L_{\mathrm{d}} - L_{\mathrm{q}}) i_{\mathrm{d}} i_{\mathrm{q}}), \tag{2}$$

where i_{d}, i_{q}, and u_{d}, u_{q} are the current and voltage of the stator d-q axis, respectively. L_{d} and L_{q} are the stator d-q-axis inductance, respectively; R is the stator resistance; ψ_{f} is the permanent magnet flux linkage; ω is the electrical angular velocity; T_{e} is the electromagnetic torque, and p is the pairs of poles.

From Equation (2), it can be seen that in addition to the excitation torque generated by the permanent magnet, there is the reluctance torque generated by the d-q axis inductances in the electromagnetic torque, and the magnitude of the electromagnetic torque outputted by the motor depends on i_{d} and i_{q}. As shown in Figure 1, the angle between the stator current I_{s} and the d-axis is called the current vector angle β. The calculation relationship between I_{s}, i_{d}, i_{q}, and β is shown in Equation (3).

$$\begin{cases} i_{\mathrm{d}} = I_{\mathrm{s}} \cos\beta \\ i_{\mathrm{q}} = I_{\mathrm{s}} \sin\beta \end{cases}, \tag{3}$$

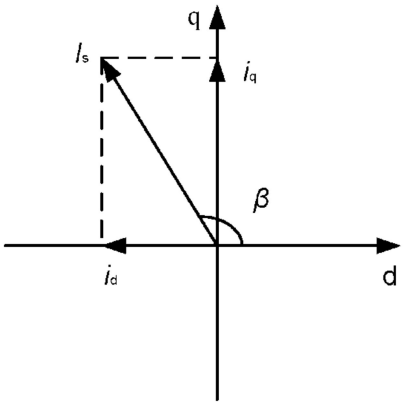

Figure 1. The current vector relationship in the d-q coordinate system.

By substituting Equation (3) into the torque formula (Equation (2)), we obtain the electromagnetic torque calculation formula expressed by the stator current and the current angle as shown in Equation (4).

$$T_{\mathrm{e}} = 1.5p(\psi_{\mathrm{f}} I_{\mathrm{s}} \sin\beta + (L_{\mathrm{d}} - L_{\mathrm{q}}) I_{\mathrm{s}}^2 \sin\beta\cos\beta), \tag{4}$$

The MTPA current angle can be obtained using Equation (5).

$$\beta = \arccos\frac{-\psi_{\mathrm{f}} + \sqrt{\psi_{\mathrm{f}}^2 + 8(L_{\mathrm{d}} - L_{\mathrm{q}})^2 I_{\mathrm{s}}^2}}{4(L_{\mathrm{d}} - L_{\mathrm{q}}) I_{\mathrm{s}}}, \tag{5}$$

To realize MTPA, the proportion relationship between i_{d} and i_{q} must be reasonably distributed to achieve the maximum electromagnetic torque output in the IPMSM.

3. MTPA Control Based on Virtual Signal Injection

3.1. Determining the Torque by Using a High-Frequency Signal

When the motor is in a stable operation state, the differential term in the d-q axis voltage equation (Equation (1) can be regarded as zero, and the d-q axis voltage can be expressed as follows:

$$\begin{cases} L_{\mathrm{q}} = -\frac{u_{\mathrm{d}} - Ri_{\mathrm{d}}}{i_{\mathrm{q}}\omega} \\ \psi_{\mathrm{f}} = \frac{u_{\mathrm{q}} - Ri_{\mathrm{q}}}{\omega} - L_{\mathrm{d}} i_{\mathrm{d}} \end{cases}, \tag{6}$$

Substituting Equation (6) into Equation (2), we obtain

$$T_{\mathrm{e}} = \frac{3}{2} p\left(\frac{u_{\mathrm{q}} - Ri_{\mathrm{q}}}{\omega} - L_{\mathrm{d}} i_{\mathrm{d}} + \left(\frac{u_{\mathrm{d}} - Ri_{\mathrm{d}}}{i_{\mathrm{q}}\omega} + L_{\mathrm{d}}\right) i_{\mathrm{d}}\right) i_{\mathrm{q}}, \tag{7}$$

After calculating the re-expressed electromagnetic torque, a high-frequency sinusoidal small-signal $\Delta\beta$ (Equation (8) is mathematically injected into the current angle β in Equation (3); the corresponding d-q axis currents i_{d} and i_{q} can be expressed as Equation (9), where ω_{h} is the injection frequency of the high-frequency signal.

$$\Delta\beta = A\sin(\omega_{\mathrm{h}} t), \tag{8}$$

$$\begin{cases} i_{\mathrm{d}}^{\mathrm{h}} = I_{\mathrm{s}}\cos(\beta + \Delta\beta) \\ i_{\mathrm{q}}^{\mathrm{h}} = I_{\mathrm{s}}\sin(\beta + \Delta\beta) \end{cases}, \tag{9}$$

The injection frequency ω_{h} in the high-frequency sinusoidal small-signal $\Delta\beta$ must be greater than the bandwidth of the outer speed loop, and the frequency ω_{h} must be much smaller than the inverter switching frequency to ensure the integrity of the injected signal. Moreover, the amplitude A must be sufficiently small to ensure that the injected high-frequency signal is not affected by the speed change.

Substituting Equations (8) and (9) into Equation (7), the torque expression containing high-frequency information can be obtained as shown in Equation (10).

$$T_{\mathrm{e}}^{\mathrm{h}}(\beta + A\sin(\omega_{\mathrm{h}} t)) = \frac{3}{2} p\left(\frac{u_{\mathrm{q}} - Ri_{\mathrm{q}}}{\omega} - L_{\mathrm{d}}(i_{\mathrm{d}} - i_{d}^{\mathrm{h}}) + \frac{u_{\mathrm{d}} - Ri_{\mathrm{d}}}{i_{\mathrm{q}}\omega} i_{\mathrm{d}}^{\mathrm{h}}\right) i_{\mathrm{q}}^{\mathrm{h}}, \tag{10}$$

From Equation (10), it can be seen that to achieve accurate torque information estimation, only the L_{d} information is needed. Although ($\psi_{\mathrm{f}} + L_{\mathrm{d}} i_{\mathrm{d}}$) varies with temperature and d-q axis current, it can be considered constant during signal injection because $(u_{\mathrm{q}} - Ri_{\mathrm{q}})/\omega$ and $(Ri_{\mathrm{d}} - u_{\mathrm{d}})/i_{\mathrm{q}}\omega$ represent parameter information ($\psi_{\mathrm{f}} + L_{\mathrm{d}} i_{\mathrm{d}}$) and L_{q}. Thus, ($\psi_{\mathrm{f}} + L_{\mathrm{d}} i_{\mathrm{d}}$) can be considered constant during signal injection, and no high-frequency signal is injected into the stator current angle contained in i_{d} and i_{q}.

3.2. Processing of High-Frequency Torque Signals

The expression of the torque model containing high-frequency information expanded according to Taylor's formula is shown in Equation (11).

$$T_{\mathrm{e}}^{\mathrm{h}}(\beta + A\sin(\omega_{\mathrm{h}} t)) = T_{\mathrm{e}}(\beta) + \frac{\partial T_{\mathrm{e}}}{\partial\beta} A\sin(\omega_{\mathrm{h}} t) + \frac{\partial}{\partial\beta}\left(\frac{\partial T_{\mathrm{e}}}{\partial\beta}\right) A^2 \sin^2(\omega_{\mathrm{h}} t) + \cdots, \tag{11}$$

Because the injected high-frequency signal amplitude A is sufficiently small, the first-order term in Equation (11) is the main part of the torque change information, and the higher-order terms (above the second-order term) have little influence on the torque change and can be ignored. Further, the quadratic term in the Taylor expansion can be expanded

into the sum of the constant term and the double frequency term of the injected signal by using trigonometric functions as follows:

$$\frac{\partial}{\partial\beta}\left(\frac{\partial T_e}{\partial\beta}\right)A^2\sin^2(\omega_h t) = \frac{1}{2}\frac{\partial}{\partial\beta}\left(\frac{\partial T_e}{\partial\beta}\right)A^2(1-\cos(2\omega_h t)), \tag{12}$$

As previously mentioned, the core principle of MTPA implementation is to make the first-order partial derivative of torque to current angle $\partial T_e/\partial\beta = 0$. Next, we need some methods and filters to perform the signal processing of the clutter in Equation (11), as shown in Figure 2. Finally, the part containing only $\partial T_e/\partial\beta$ term is obtained to realize MTPA control.

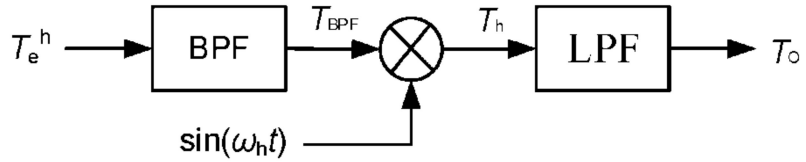

Figure 2. Extraction of virtual signal injection MTPA criterion.

In Figure 2, the torque signal containing high-frequency components is passed through the band-pass filter (BPF) to obtain only the fundamental frequency component of the injected signal. The BPF is a device that allows certain frequency bands of waves to pass while blocking other frequency bands. The center frequency of the BPF is ω_h, and all the signal components of other frequencies are filtered out. Next, after multiplying with $\sin(\omega_h t)$, the quadratic component of $\sin(\omega_h t)$ is obtained, and Equation (13) is obtained by expanding Equation (12).

$$\frac{\partial T_e}{\partial\beta}A\sin^2(\omega_h t) = \frac{1}{2}\frac{\partial T_e}{\partial\beta}A(1-\cos(2\omega_h t)), \tag{13}$$

Equation (13) consists of a constant term containing only $\partial T_e/\partial\beta$ and the double frequency term of the injected signal. Finally, the first-order deviation of the electromagnetic torque is obtained after the double frequency term is filtered out by the low-pass filter (LPF) (Figure 2). The action of the LPF is to suppress the high-frequency of waves and allow the low-frequency of waves to pass.

To sum up, in the proposed method, the calculation formula of electromagnetic torque is re-expressed as follows: by injecting a high-frequency, small-amplitude current angle signal, the high-frequency signal of the current is included in the expression of the electromagnetic torque. Next, the torque model containing high-frequency information is expanded according to the Taylor formula, $\partial T_e/\partial\beta$ is obtained after multiple filtering, and the integral result is taken as the given value of the reference current angle. If it does not work at the MTPA point at this time and $\partial T_e/\partial\beta \neq 0$, the integrator will continue to integrate and adjust the current angle until it works at the MTPA point; at this time, $\partial T_e/\partial\beta = 0$, and the reference current angle remains unchanged from the previous state due to the zero input to the integrator, and the motor continues to run at the MTPA point.

3.3. Error Analysis and Application Occasions

Compared with the formula calculation method, the VSIC method involves fewer motor parameters; thus, the influence of parameter changes on the MTPA control accuracy is greatly reduced, high-frequency signals do not need to be injected into the motor, and the torque to the current angle change rate can be obtained through signal processing technology to achieve complete MTPA control. However, there is still a certain amount of error in the MTPA angle obtained using this method. From Equation (10), it can be seen that to accurately obtain the change rate $\partial T_e/\partial\beta$ of the electromagnetic torque to the stator current angle, it is necessary to replace the permanent magnet flux linkage ψ_f, the direct-axis inductance L_d, and the quadrature-axis inductance L_q. However, ψ_f and $L_d i_d$ are

coupled in the motor parameter estimation formula (Equation (6) and cannot be extracted separately. Therefore, the error of the direct-axis inductance L_d is ignored.

When the reluctance torque ratio of IPMSM is large, $L_d(i_d - {i_d}^h)$ in Equation (10) can be ignored. The approximate calculation formula (Equation (14) further ignores the influence of L_d change so that the MTPA control strategy based on VSIC is not affected by any parameters; thus, it is simpler and more convenient.

$$T_e^h(\beta + A\sin(\omega_h t)) = \frac{3}{2}p(\frac{u_q - Ri_q}{\omega} + \frac{u_d - Ri_d}{i_q\omega}i_d^h)i_q^h, \quad (14)$$

However, in the IPMSM with a small proportion of reluctance torque, $L_d(i_d - {i_d}^h)$ cannot be ignored; otherwise, the error between the automatically found MTPA point and the correct MTPA point in the algorithm will be too large, resulting in the failure of optimization. In the simulation, by setting an IPMSM with a small reluctance torque, the optimization results obtained using the exact torque calculation formula (Equation (10) are compared with those obtained using the approximate torque calculation formula (Equation (14)), and the simulation data are recorded (Figure 3). The optimization effect is better in the IPMSM with a small reluctance torque using the accurate calculation formula.

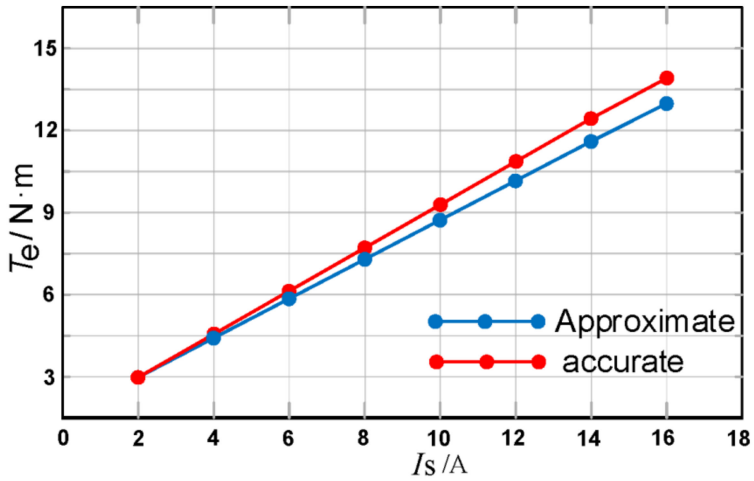

Figure 3. Comparison of simulation results obtained using different torque calculation formulas.

Based on the above analysis and simulation verification, for the IPMSM with a large proportion of reluctance torque, the approximate torque calculation formula can be used to ignore the influence of the d-axis inductance and thus simplify the control system. When the reluctance torque is small, the change in the inductance term cannot be ignored; otherwise, the control accuracy will be reduced, and the optimization will fail. Therefore, the value of the d-axis inductance must be obtained in real-time.

4. MTPA Control Based on Inductance Identification

4.1. Model Reference Adaptive System

As previously discussed, for realizing high-precision control by using the MTPA virtual signal injection method in an IPMSM with a small reluctance torque, the influence of the inductance term cannot be ignored, and the d-axis inductance of the motor must be known. Therefore, the online identification of the inductance must be realized using the MRAS system, which consists of a reference model, an adjustable model, and a parameter adaptive law. The reference model specifies the performance of the system, and its output represents the desired ideal output curve of the closed-loop control system, which shows the main features of MRAS. The actual motor is set as the reference model and is inputted at the same voltage as the adjustable model; the error signal e is generated by comparing the current output in real-time. The parameters of the adjustable model are modified

using appropriate adaptive laws. When the error signal decays to 0, the parameters of the adjustable model converge to the actual value. The structure of MRAS is shown in Figure 4.

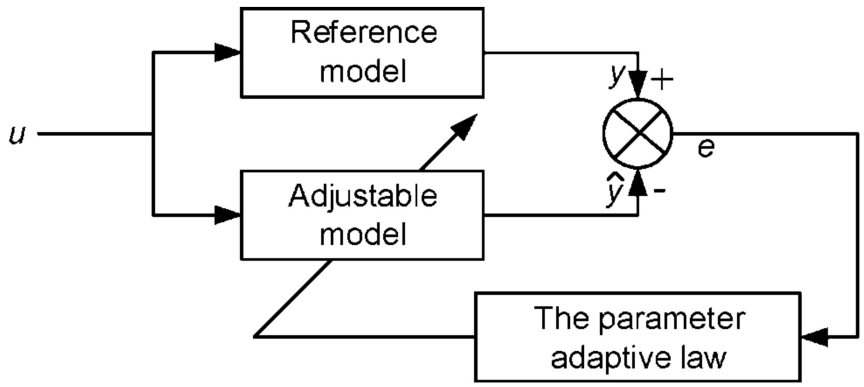

Figure 4. Block diagram of the model reference adaptive system.

For the IPMSM system, the input is $u = [u_d u_q\ ]^T$, the output of the reference model is $y = i = [i_d i_q\ ]^T$, the output of the adjustable model is $\hat{y} = \hat{i} = [\hat{i}_d \hat{i}_q\ ]^T$, and the output quantity error is $e = i - \hat{i}$.

The adaptive law of the model reference adaptive system is a vital part of the system. Currently, the following three common methods are available for determining the appropriate adaptive law:

1. Design method based on local parameter optimization theory (MIT method);
2. Design method based on Lyapunov function;
3. Design method based on ultra-stable and positive dynamic theory (Popov super stability theory).

Among the three methods, the MIT method causes significant defects, and the stability of the adaptive system is not known. In contrast, although the Lyapunov function-based design method is feasible for designing a stable model reference adaptive system, the Lyapunov function has no definite form and includes different types. The Popov super stability theory involves using the reverse solution of the Popov integral inequality to construct the parameter adaptation rate. Because the solution process is concise, it is widely used in the construction of the parameter adaptation rate of the MRAS system.

To sum up, in this study, the design method based on the Popov super stability theory was adopted to construct the parameter adaptation rate of the MRAS system. For the MRAS system to reach an asymptotically stable state, the following two conditions of the Popov law of super stability must be satisfied:

1. The conditions of the Popov integral inequality must be satisfied according to the nonlinear time-varying feedback loop;
2. An appropriate gain matrix M must be selected to ensure that the transfer function matrix of the linear steady forward loop is strictly positive and real.

4.2. Reference Model of the IPMSM System

According to Equation (1), the state space equation of the IPMSM system can be described as follows:

$$\begin{bmatrix} \frac{di_d}{dt} \\ \frac{di_q}{dt} \end{bmatrix} = \begin{bmatrix} -\frac{R_s}{L_d} & \frac{L_q}{L_d}\omega \\ -\frac{L_d}{L_q}\omega & -\frac{R_s}{L_q} \end{bmatrix} \begin{bmatrix} i_d \\ i_q \end{bmatrix} + \begin{bmatrix} \frac{1}{L_d} & 0 \\ 0 & \frac{1}{L_q} \end{bmatrix} \begin{bmatrix} u_d \\ u_q \end{bmatrix} + \begin{bmatrix} 0 \\ -\frac{\psi_f}{L_q}\omega \end{bmatrix}, \tag{15}$$

Equation (15) is considered as the reference model of IPMSM in the MRAS and is simplified as follows:

$$\dot{i} = Ai + Bu + C, \tag{16}$$

where $A = \begin{bmatrix} -\frac{R_s}{L_d} & \frac{L_q}{L_d}\omega \\ -\frac{L_d}{L_q}\omega & -\frac{R_s}{L_q} \end{bmatrix}$, $B = \begin{bmatrix} \frac{1}{L_d} & 0 \\ 0 & \frac{1}{L_q} \end{bmatrix}$, and $C = \begin{bmatrix} 0 \\ -\frac{\psi_f}{L_q}\omega \end{bmatrix}$.

4.3. Adjustable Model of the IPMSM System

In the identification process, the motor speed ω and rotor flux linkage ψ_f are assumed to be constant; thus, the parameter adjustable model can be constructed from the following reference model:

$$\dot{\hat{i}} = \hat{A}\hat{i} + \hat{B}u + \hat{C} - Me, \tag{17}$$

where $\hat{A} = \begin{bmatrix} -\frac{R_s}{\hat{L}_d} & \frac{\hat{L}_q}{\hat{L}_d}\omega \\ -\frac{\hat{L}_d}{\hat{L}_q}\omega & -\frac{R_s}{\hat{L}_q} \end{bmatrix}$, $\hat{B} = \begin{bmatrix} \frac{1}{\hat{L}_d} & 0 \\ 0 & \frac{1}{\hat{L}_q} \end{bmatrix}$, $\hat{C} = \begin{bmatrix} 0 \\ -\frac{\psi_f}{\hat{L}_q}\omega \end{bmatrix}$, M is the gain matrix, and $M = \begin{bmatrix} -m_{11} & -m_{12} \\ m_{21} & -m_{22} \end{bmatrix}$.

The error equation of the model-referenced adaptive system is obtained by subtracting the adjustable model from the following reference model:

$$\dot{e} = (A + M)e + \Delta A\hat{i} + \Delta Bu + \Delta C, \tag{18}$$

where $\Delta A = A - \hat{A}$, $\Delta B = B - \hat{B}$, and $\Delta C = C - \hat{C}$.

4.4. Model Reference Adaptive System Parameter Identifier Design

The error equation of MRAS is transformed into an equivalent nonlinear time-varying feedback system that consists of a linear steady-state forward loop and a nonlinear time-varying feedback loop.

Let $w = -(\Delta A\hat{i} + \Delta Bu + \Delta C)$. Accordingly, the parameter identification model formula (Equation (18)) can be rewritten as follows:

$$\dot{e} = (A + M)e - w, \tag{19}$$

The equivalent nonlinear time-varying feedback system can be derived from Equation (19) and is shown in Figure 5, where $\varphi(e)$ is the adaptive law with respect to the parameter matrices A, B, and C.

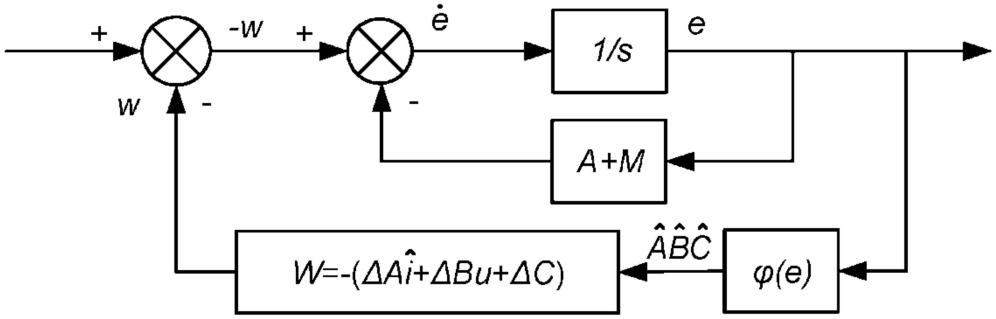

Figure 5. Equivalent nonlinear time−varying feedback system.

The nonlinear time−varying feedback system constructed above must satisfy the conditions of the Popov integral inequality. The Popov integral inequality is given as follows:

$$\eta(0, t_1) = \int_0^{t_1} e^{\mathrm{T}} w dt \geq -\gamma^2, \tag{20}$$

In Equation (20), for any $t \geq 0$, γ is a finite constant independent of t.

Taking L_d and L_q as identification objects and substituting w into Equation (20), we obtain the follows:

$$\eta(0,t_1) = \int_0^{t_1} e^T w dt = \int_0^{t_1} (-e^T \Delta A \hat{i} - e^T \Delta B u - e^T \Delta C) dt \geq -\gamma^2, \tag{21}$$

Equation (21) can be decomposed into the following three formulas:

$$\eta_1(0,t_1) = -\int_0^{t_1} e^T \Delta A \hat{i} dt \geq -{\gamma_1}^2, \tag{22}$$

$$\eta_2(0,t_1) = -\int_0^{t_1} e^T \Delta B u dt \geq -{\gamma_2}^2, \tag{23}$$

$$\eta_3(0,t_1) = -\int_0^{t_1} e^T \Delta C dt \geq -{\gamma_3}^2, \tag{24}$$

According to the Popov super stability theory, as long as Equations (22)–(24) are satisfied, the nonlinear feedback system remains stable. Then, the adaptive law can be derived from Equations (22)–(24). Because Equation (23) does not contain the inductive coupling term of the quadrature axis, the adaptive law of the identification of the quadrature axis inductance can be deduced using Equation (23). Thus, Equation (23) can be transformed into Equation (25) as follows:

$$\eta_2(0,t_1) = -\int_0^{t_1} (i_d - \hat{i}_d)(\frac{1}{L_d} - \frac{1}{\hat{L}_d}) u_d + (i_q - \hat{i}_q)(\frac{1}{L_q} - \frac{1}{\hat{L}_q}) u_q dt \geq -{\gamma_2}^2, \tag{25}$$

Next, Equation (25) can be decomposed into Equations (26) and (27) as follows:

$$\eta_{21}(0,t_1) = \int_0^{t_1} (i_d - \hat{i}_d)(\frac{1}{\hat{L}_d} - \frac{1}{L_d}) u_d dt \geq -{\gamma_{21}}^2, \tag{26}$$

$$\eta_{22}(0,t_1) = \int_0^{t_1} (i_q - \hat{i}_q)(\frac{1}{\hat{L}_q} - \frac{1}{L_q}) u_q dt \geq -{\gamma_{22}}^2, \tag{27}$$

The PI adaptive law about L_d is usually expressed as follows:

$$\frac{1}{\hat{L}_d} = \frac{1}{L_d} + f_1(t) + \int_0^t f_1(\tau) d\tau, \tag{28}$$

Only the adaptation law of the direct-axis inductance identification is analyzed; the derivation process of the quadrature-axis adaptation law is similar. Substituting Equation (28) into Equation (26), $\eta_{21}(0,t_1)$ can be further decomposed into the following two sub-inequalities:

$$\eta_{211}(0,t_1) = \int_0^{t_1} u_d (i_d - \hat{i}_d) f_1(t) dt \geq -{\gamma_{211}}^2, \tag{29}$$

$$\eta_{212}(0,t_1) = \int_0^{t_1} u_d (i_d - \hat{i}_d) \int_0^t f_1(\tau) d\tau dt \geq -{\gamma_{212}}^2, \tag{30}$$

From Equations (29)–(30), the PI adaptive law of parameter L_d can be obtained as follows:

$$\frac{1}{\hat{L}_d} = \frac{1}{L_d} + (k_1 + \frac{1}{\tau_1 s}) u_d (i_d - \hat{i}_d), \tag{31}$$

where k_1 and τ_1 are the proportional and integral coefficients of the L_d adaptive law, respectively.

Similarly, the adaptive law of L_q can be obtained as follows:

$$\frac{1}{\hat{L}_q} = \frac{1}{L_q} + (k_2 + \frac{1}{\tau_2 s}) u_q (i_q - \hat{i}_q), \tag{32}$$

where k_2 and τ_2 are the proportional and integral coefficients of the L_q adaptive law, respectively.

The overall structure of the IPMSM MTPA drive control system is illustrated in Figure 6.

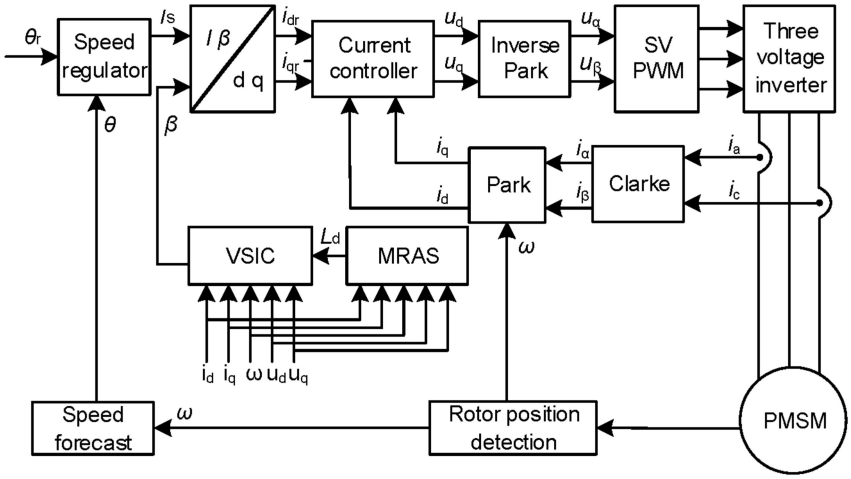

Figure 6. Interior permanent magnet synchronous motor MTPA drive control system.

5. Simulation Results and Analysis

In this study, the simulation model of the IPMSM drive control system was established in the MATLAB/Simulink software environment, and the simulation tests and analysis were performed. The main parameters of the motor are presented in Table 1. The main parameters of the VSIC-type MTPA control method based on inductance identification are presented in Table 2.

Table 1. Main parameters of the IPMSM in the simulation.

Main Parameters	Rated Value
Rated speed	1000 r/min
Rated torque	10 N·m
q-axis inductance	12 mH
d-axis inductance	5.5 mH
The rotor flux	0.1827 Wb
Pairs of poles	4
The moment of inertia	0.003 kg·m^2

Table 2. Main parameters of the VSIC-type MTPA control method based on inductance identification in the simulation.

Main Parameters	Numerical Value
Injected signal amplitude A	0.05 A
Injected signal frequency ω_h	300 Hz
MRAS L_d PI proportional coefficient k_1	0.01
MRAS L_d PI integral coefficient τ_1	10.25
MRAS L_q PI proportional coefficient k_2	0.01
MRAS L_q PI integral coefficient τ_2	1.02

5.1. MTPA Operation Effectiveness Analysis

The motor was run at 1000 r/min, 10 N·m. When the motor was in a stable operation state, the stator current angle gradually increased from 1.57 rad to 2.14 rad. Figure 7 expresses the corresponding waveform changes of the stator current amplitude and $\partial T_e/\partial\beta$ when the stator current angle gradually increases with time.

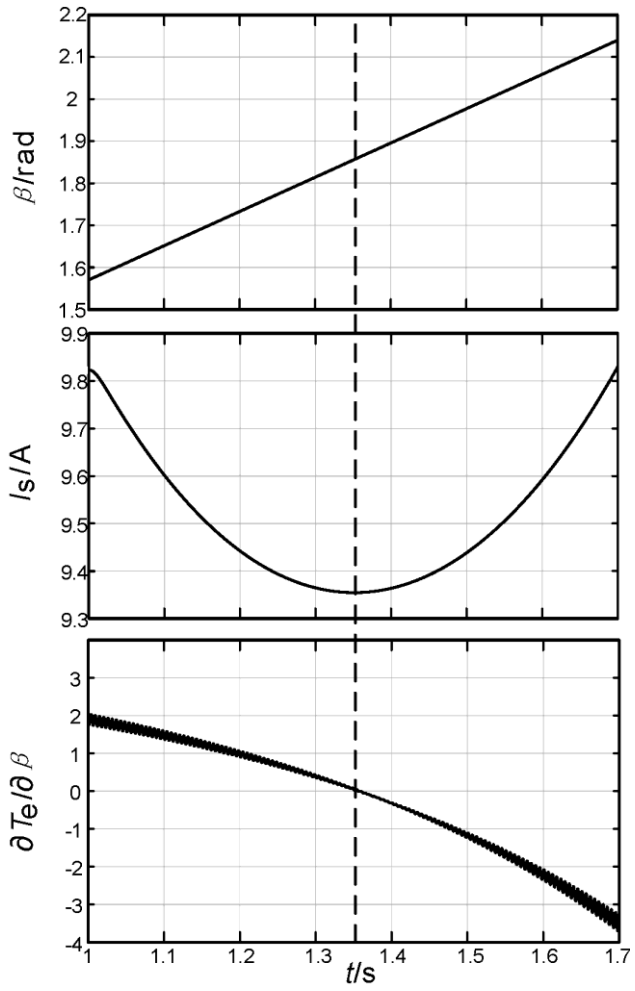

Figure 7. Stator current angle, current amplitude, and $\partial T_e/\partial\beta$ waveform.

The stator current amplitude first decreased and then increased, reaching the minimum at t = 1.35 s. The minimum stator current RMS was 9.37 A, and the corresponding MTPA angle was approximately 1.85 rad, which is in line with the expected actual value. The MTPA points were the same. In addition, the corresponding torque versus current angular change rate revealed that when $\beta \leq \beta_{\mathrm{MTPA}}$, $\partial T_e/\partial\beta \geq 0$; when $\beta \geq \beta_{\mathrm{MTPA}}$, $\partial T_e/\partial\beta \leq 0$; when $\beta = \beta_{\mathrm{MTPA}}$, $\partial T_e/\partial\beta = 0$. This result is consistent with the theoretical analysis, thus, proving that the proposed method can effectively track the MTPA current angle.

Under the condition of no load, the motor reached the given speed value of 1000 r/min after t = 0.06 s. When the motor reached a stable running state, a load torque of 10 N·m was added at t = 1.5 s. The command and feedback tracking performance of the motor speed and load torque, the motor torque tracking performance of the current angle change rate, and the command and feedback of the stator vector angle were compared to demonstrate the improved algorithm accuracy.

After a sudden load was applied, the speed decreased, and the system quickly returned to the steady state (Figure 8), thus, showing that the proposed method has a good speed tracking effect. After the system started, the speed tracked the command very well. The overshoot was only 8 r/min (0.8%), the maximum speed drop after the addition of load was only 12 r/min (1.2%), and it quickly returned to the steady state. The simulation results show that the speed loop controlled by MTPA has good dynamic and steady-state performance and strong anti-load disturbance capability.

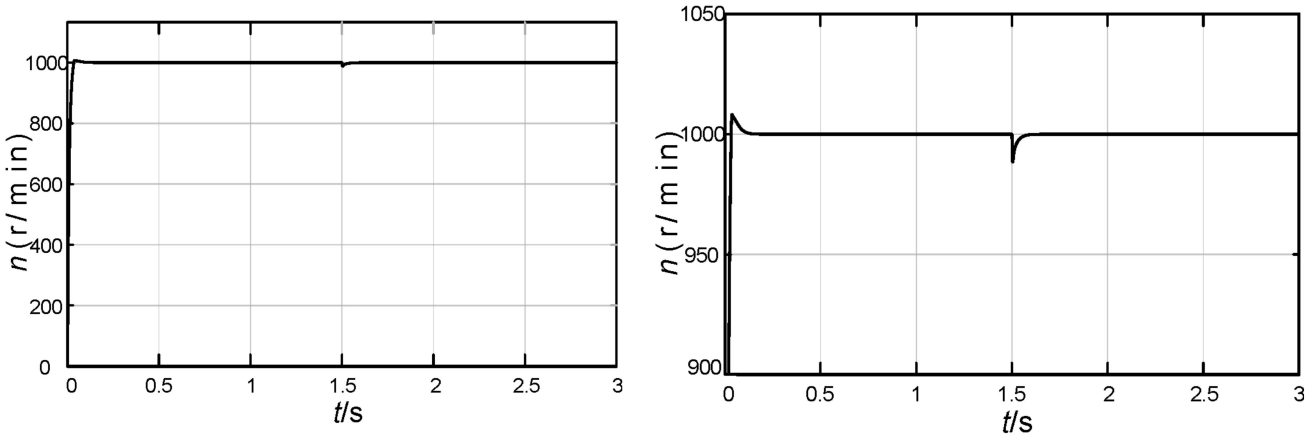

(**a**) (**b**)

Figure 8. Waveform of rotational speed. (**a**) Waveform of rotational speed; (**b**) Zoomed waveform of rotational speed.

Figure 9 shows that IPMSM can provide a large torque when starting. The motor load torque was 10 N·m, and the electromagnetic torque was 10.32 N·m, indicating that the motor has good accuracy. When the rated speed and rated load were used, the minimum stator current value was 9.37 A, and the optimal stator current value was almost the same, thereby demonstrating very good accuracy.

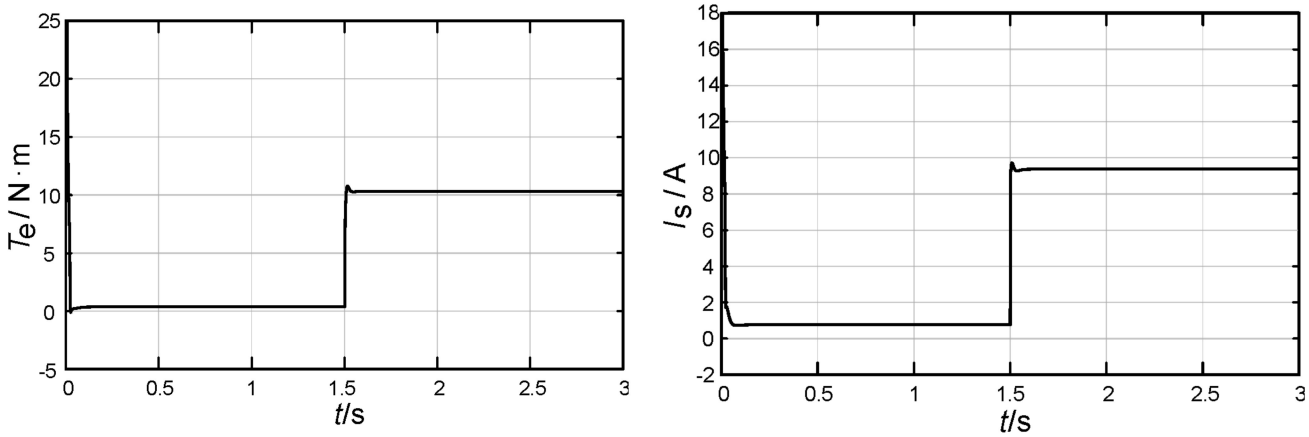

(**a**) (**b**)

Figure 9. Torque and current waveforms. (**a**) Torque waveform; (**b**) Stator current waveform.

Figure 10 shows that at the moment of sudden torque change, the method responded immediately to make the MTPA angle converge, and the corresponding MTPA angle after stabilization was approximately 1.85 rad, which is the same as the expected actual MTPA point. In addition, the PI regulator quickly adjusted it to a steady state of 0 to achieve the purpose of automatically tracking the MTPA angle. However, due to the influence of the filter and the integrator in the virtual signal injection method, it required 1 s to reach the steady state.

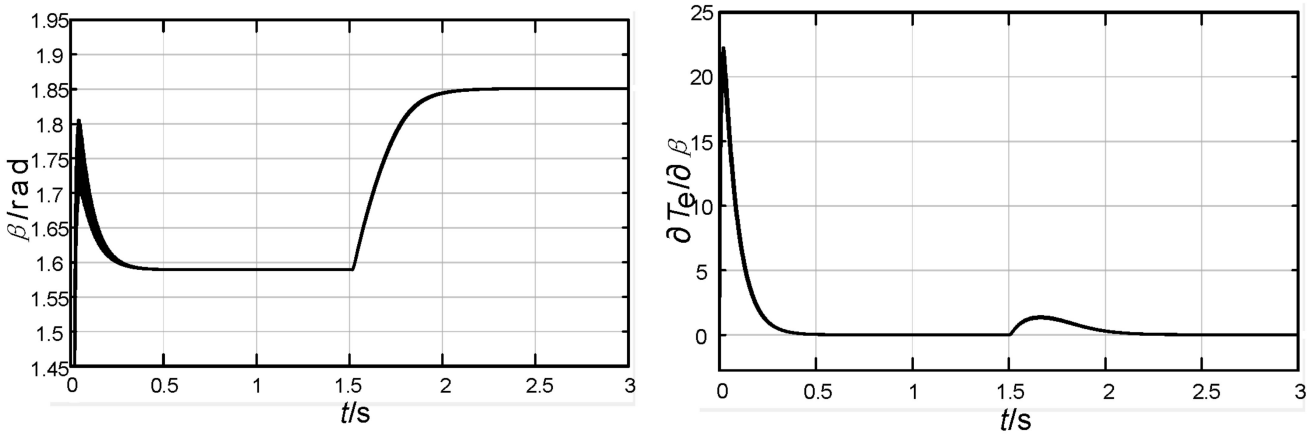

(**a**) (**b**)

Figure 10. Stator vector angle and $\partial T_e/\partial\beta$ waveform. (**a**) Stator vector angle waveform; (**b**) $\partial T_e/\partial\beta$ waveform.

5.2. MTPA Operation Accuracy Analysis

To verify that the improved virtual signal injection control (IVSIC) method MTPA control maintains strong robustness and accuracy under the parameter mismatch condition, the rated parameters of the motor model in the simulation were changed. L_d and L_q were set at 7 and 15 mH, respectively, which is an increase of approximately 1.25 times the rated value. ψ_f was set as 0.14 Wb, which is a reduction of approximately 77% of the rated value. Then, the formula control (FC) method, virtual signal injection control (VSIC) method, and IVSIC method were simulated and compared. For the IPMSM running at 1000 r/min under a load of 10 N·m, when the motor was in a stable operation state, the stator current angle gradually increased from 1.57 rad to 2.14 rad. The relational waveform of the angular change rate is shown in Figure 11.

Figure 11 shows that under this working condition (1000-r/min running speed and 10 N·m load torque), the current vector amplitude changed with the current vector angle; the minimum value was 11.12 A, and the corresponding radian was 1.99 rad. The $\partial T_e/\partial\beta$ zero-crossing point obtained using the formula calculation method was far away from the actual operating point of the MTPA, and the corresponding angle was 1.90 rad; thus, demonstrating that the control effect of the FC method is greatly affected by changes in the motor parameters and the obtained MTPA angle is not accurate. Further, the position of $\partial T_e/\partial\beta$ zero−crossing point obtained using the VSIC method was close to the actual operating point of MTPA, and the corresponding radian was 2.02 rad, but it was still inaccurate. In contrast, the $\partial T_e/\partial\beta$ zero-point obtained using the IVSIC method was very close to the actual operating point of MTPA, which shows that the proposed method has high accuracy. That is, the proposed method can more accurately track the MTPA operating point and has high accuracy.

Figures 12–14 illustrate the tracking response curves and d- and q-axis current error curves of the parameters to be identified. The value of L_d was increased to 7 mH (Figure 12), that is, approximately 1.27 times the rated value, and the value of L_q was increased to 15 mH (Figure 13), that is, approximately 1.25 times the rated value. Both parameters changed simultaneously (Figure 14); the IPMSM was run under the conditions of 1000 r/min and 10 N·m. From Figures 12–14, it can be seen that when the parameters changed, the dynamic response of the parameters to be identified had a small overshoot and converged quickly to the reference value, thereby demonstrating that the designed parameter identifier has good parameter change tracking characteristics.

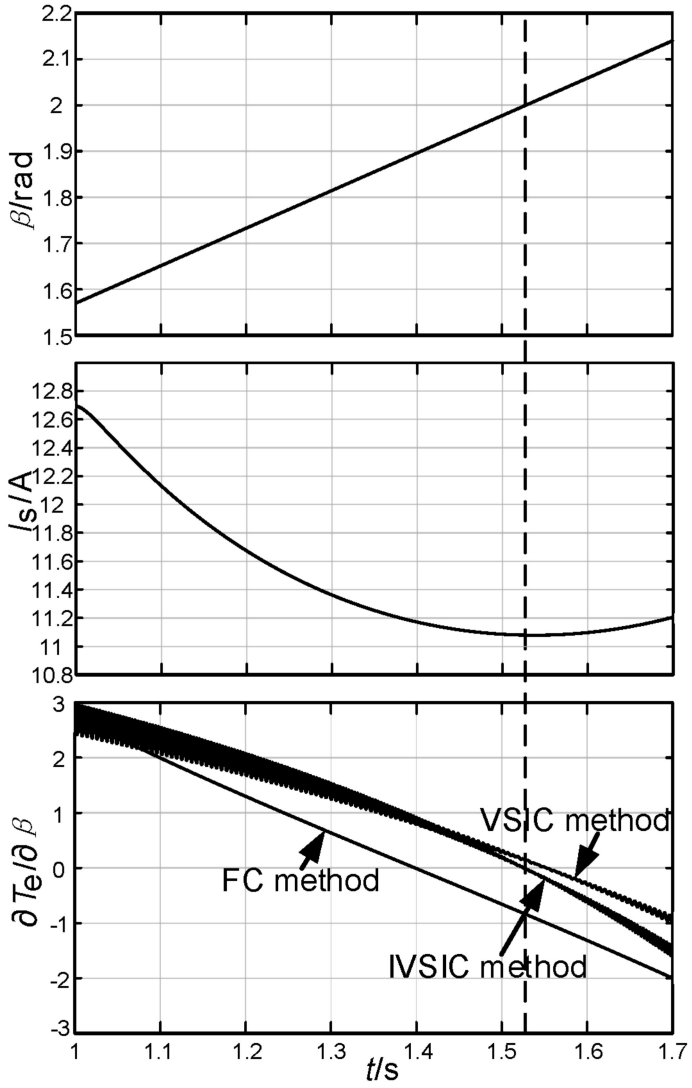

Figure 11. Stator current angle, current amplitude, and $\partial T_e/\partial\beta$ waveform.

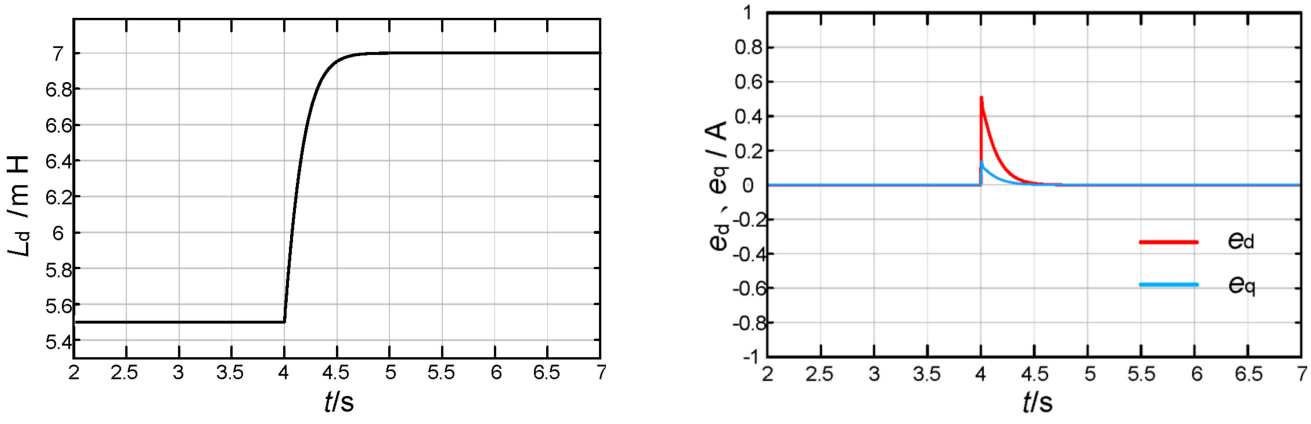

(**a**) (**b**)

Figure 12. Identification of sudden drop in d-axis inductance. (**a**) d-axis inductance identification; (**b**) d-axis and q-axis current errors.

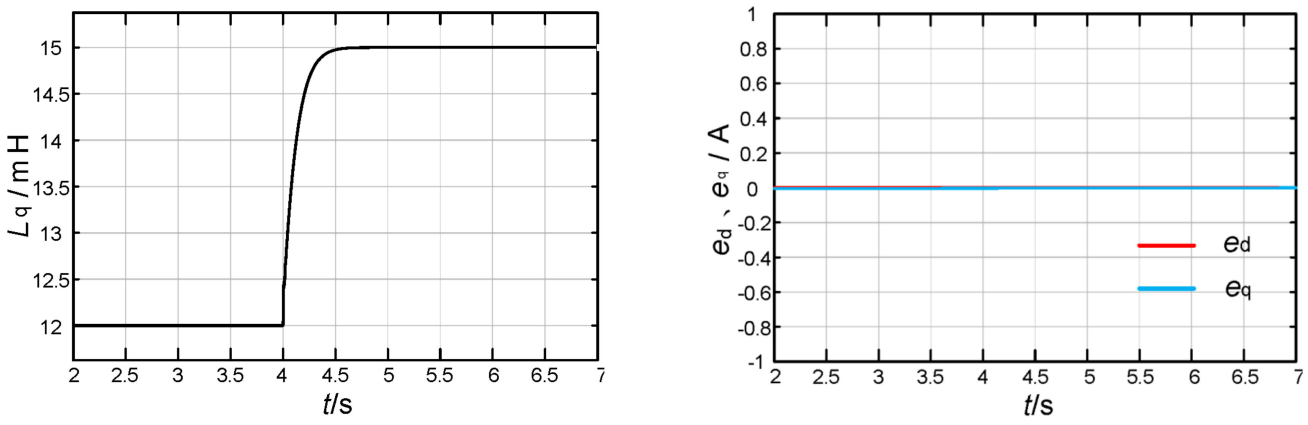

(**a**) (**b**)

Figure 13. Identification of sudden drop in q-axis inductance. (**a**) q-axis inductance identification; (**b**) d-axis and q-axis current errors.

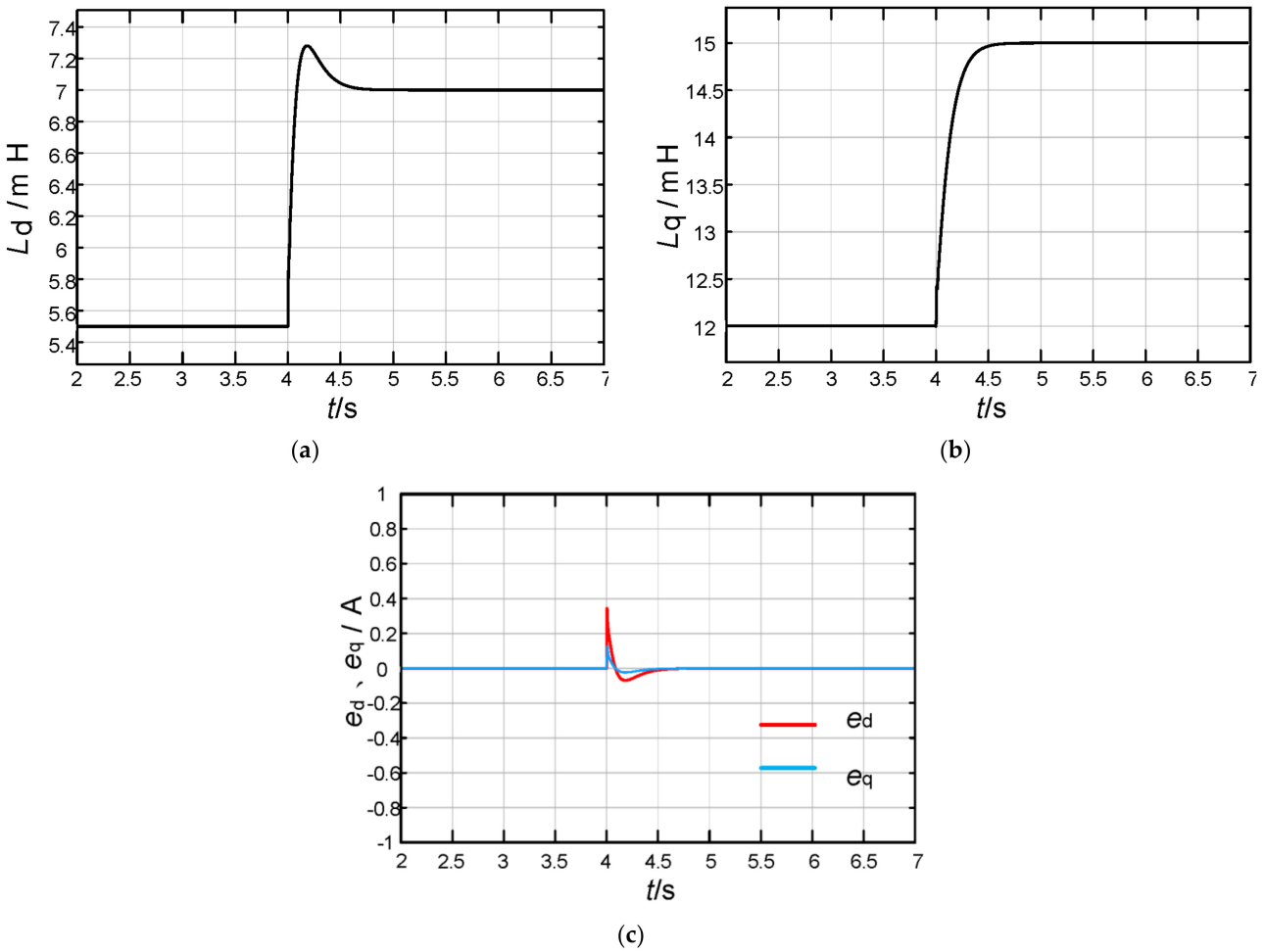

(**a**) (**b**)

(**c**)

Figure 14. Identification of simultaneous changes in L_d and L_q. (**a**) d-axis inductance identification; (**b**) q-axis inductance identification; (**c**) d-axis and q-axis current errors.

Figures 15–23, respectively, show the comparison charts of the tracking curves of the d-axis current, q-axis current, and stator current when the FC method, VSIC method, and IVSIC method were used. To highlight the influence of the change in the d-axis inductance parameter on the working efficiency of the IPMSM, three parameter changes were employed in this study. In the first case, the d-axis inductance parameter was increased from the

initial state inductance value to 7 mH, the q-axis inductance parameter was increased from the initial state inductance value to 15 mH, and the other parameters were left unchanged. In the second case, the d-axis inductance parameter was decreased from the initial state inductance value to 4 mH, the q-axis inductance parameter was decreased from the initial state inductance value to 7 mH, and the other parameters were left unchanged. In the third case, the d-axis inductance parameter was increased from the initial state inductance value to 7 mH, and the q-axis inductance parameter was decreased from the initial state inductance value to 9 mH, and the other parameters were left unchanged. For these parameter changes, the calculated expected d-axis current, q-axis current, and the operating point of the stator current changed accordingly. When the motor was run at 1000 r/min under a load torque of 10 N·m, the waveform obtained when the motor was in a stable operation state is shown in Figures 15–17.

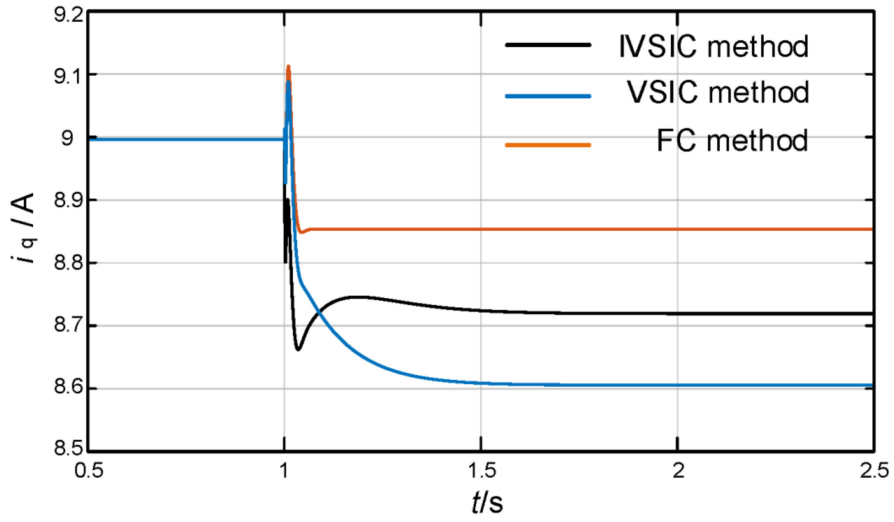

Figure 15. Comparison of tracking curves of q-axis current.

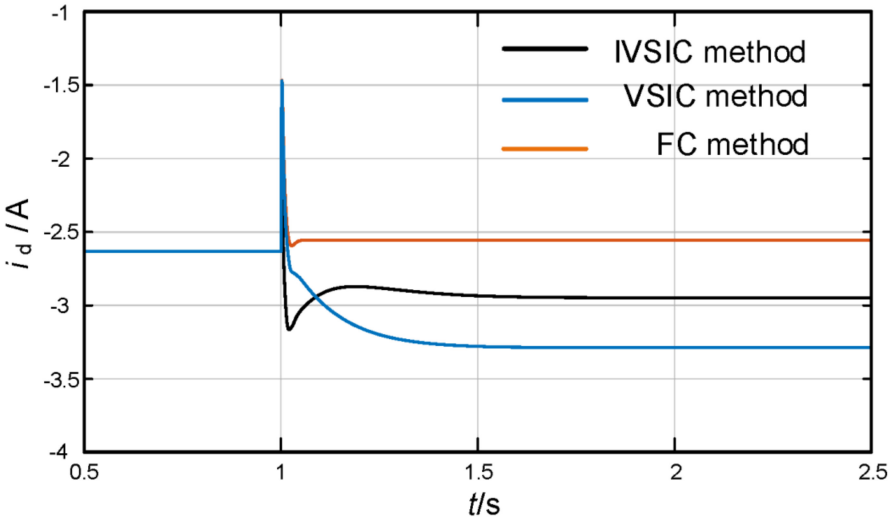

Figure 16. Comparison of tracking curves of d-axis current.

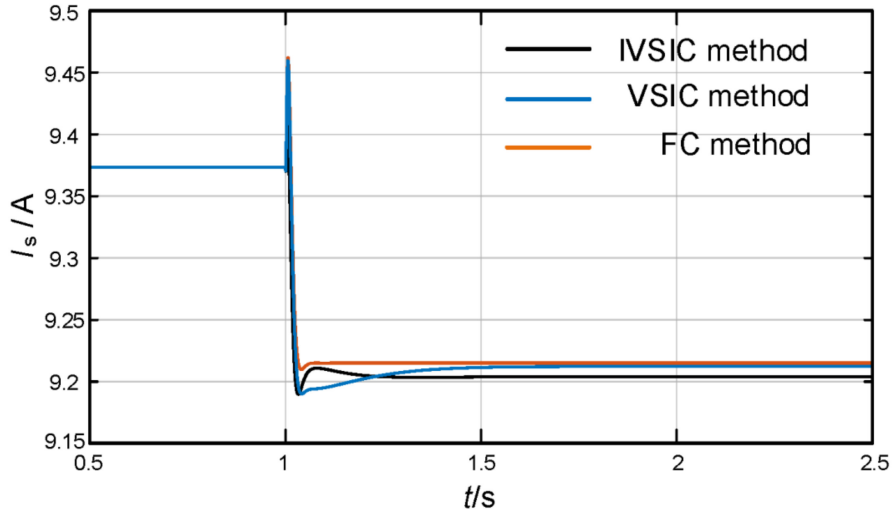

Figure 17. Comparison of tracking curves of stator current.

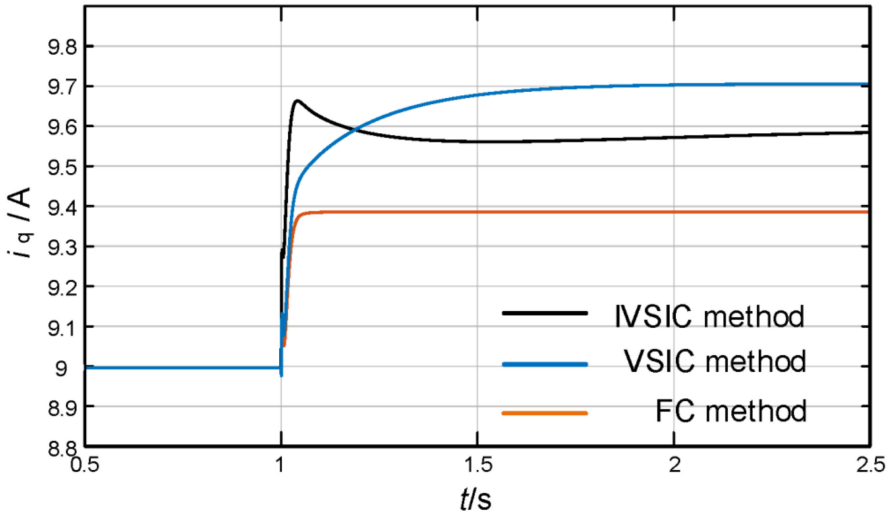

Figure 18. Comparison of tracking curves of q-axis current.

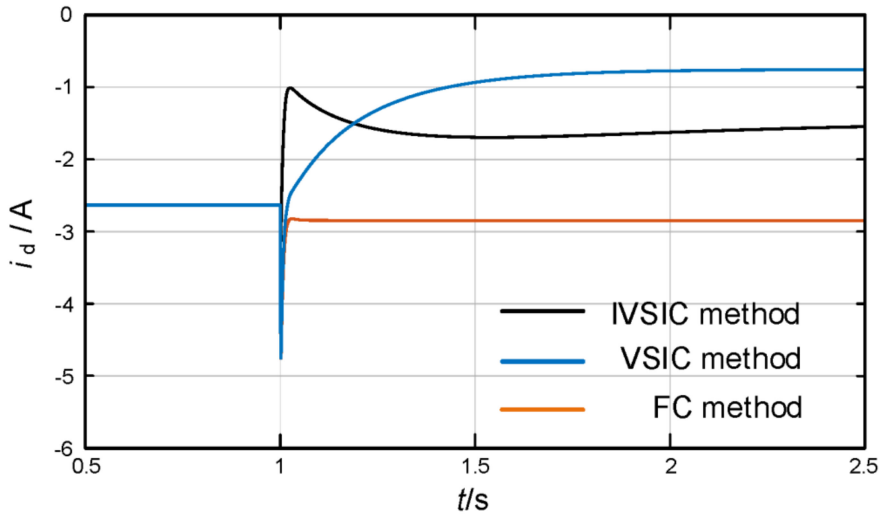

Figure 19. Comparison of tracking curves of d-axis current.

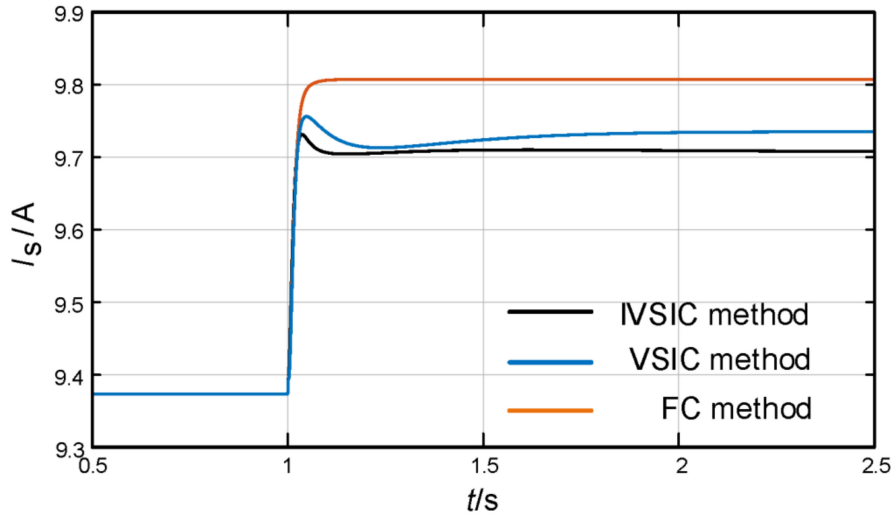

Figure 20. Comparison of tracking curves of stator current.

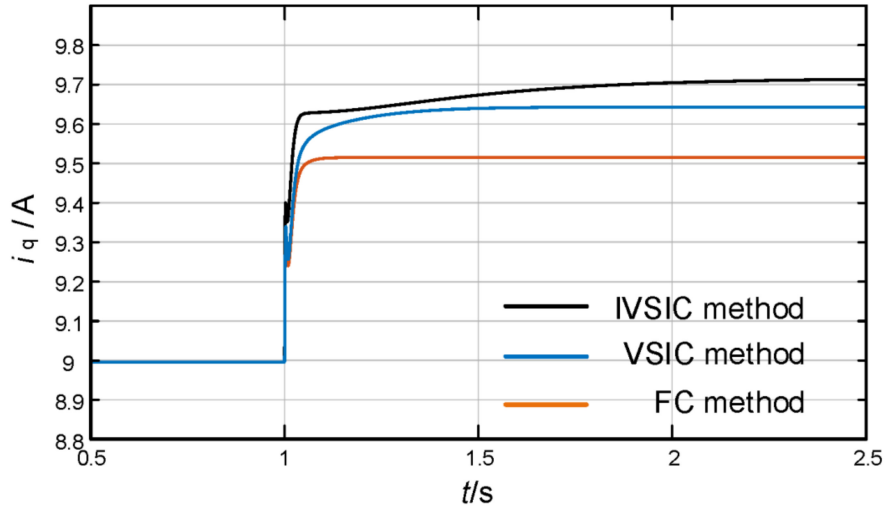

Figure 21. Comparison of tracking curves of q-axis current.

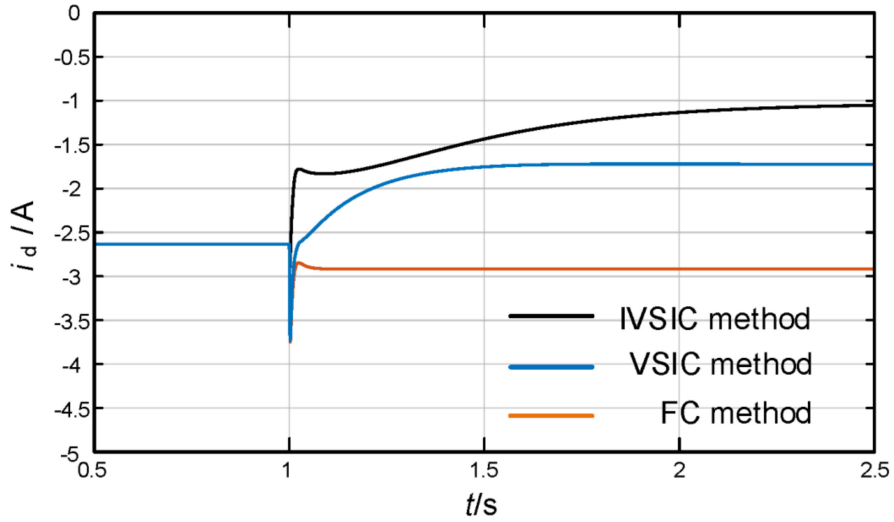

Figure 22. Comparison of tracking curves of d-axis current.

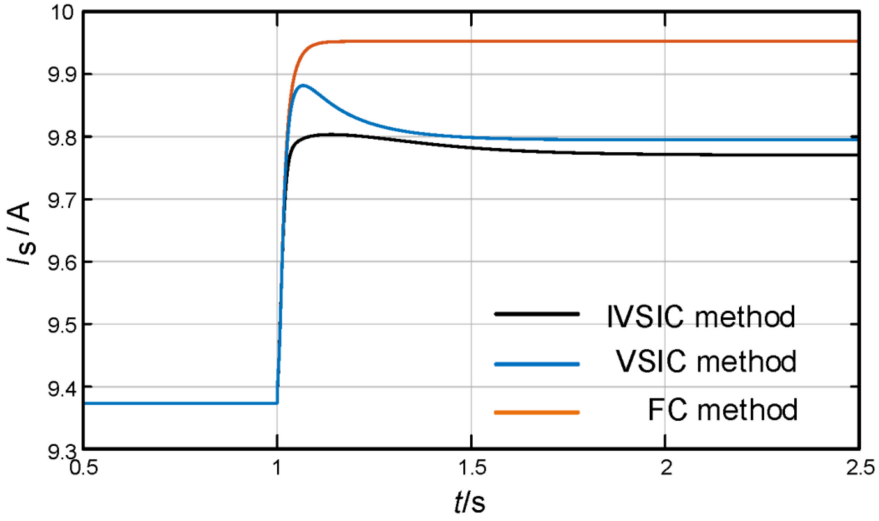

Figure 23. Comparison of tracking curves of stator current.

From Figures 15–17, it can be seen that when the inductance value was increased to 15 mH while the other parameters were left unchanged, the magnitude of the current vector changed. The largest stator current amplitude was obtained using the FC method (9.22 A), followed by the VSIC method (9.21 A) and the IVSIC method (9.20 A). The value obtained using the VSIC method was inaccurate, whereas that obtained using the IVSIC method was the same as the expected value, thus showing that the proposed control algorithm has high accuracy. Additionally, when the parameter changes, the longest current transition time t_s was obtained using the IVSIC method (0.7 s), followed by the VSIC method (0.6 s) and the FC method (0.1 s). It can be seen that the control speed drops when using the IVSIC method.

Figures 18–20 show that when the d-axis inductance parameter was decreased from the initial state inductance value to 4 mH and the q-axis inductance parameter was decreased from the initial state inductance value to 7 mH, the magnitude of the current vector changed. The largest stator current amplitude was obtained using the FC method (9.80 A), followed by the VSIC method (9.73 A) and the IVSIC method (9.71 A). The stator current amplitude obtained using the VSIC method was inaccurate, whereas that obtained using the IVSIC was the same as the expected value, thus showing that the proposed control algorithm has high accuracy. Additionally, when the parameter changes, the longest current transition time t_s was obtained using the IVSIC method (1.5 s), followed by the VSIC method (1.1 s) and the FC method (0.1 s). It can be seen that the control speed drops when using the IVSIC method.

Figures 21–23 show that when the d-axis inductance parameter was increased from the initial state inductance value to 7 mH and the q-axis inductance parameter was decreased from the initial state inductance value to 9 mH, the magnitude of the current vector changed. The largest stator current amplitude was obtained using the FC method (9.95 A), followed by the VSIC method (9.80 A) and the IVSIC method (9.77 A). The stator current amplitude obtained using the VSIC method was inaccurate, whereas that obtained using the IVSIC method was the same as the expected value, thus showing that the proposed control algorithm has high accuracy. In summary, the simulation results prove that the IVSIC method has good trajectory tracking characteristics when the parameters change. Additionally, when the parameter changes, the longest current transition time t_s was obtained using the IVSIC method (1.1 s), followed by the VSIC method (0.7 s) and the FC method (0.1 s). It can be seen that the control speed drops when using the IVSIC method.

In order to make the obtained results more significant and easier to analyze, we have organized the main data from Figures 15–23. in Table 3.

Table 3. Arrangement of the main data in Figures 15–23.

Inductor Parameter Value		FC Method				VSIC Method				IVSIC Method			
L_d (mH)	L_q (mH)	i_d (A)	i_q (A)	I_s (A)	t_s (s)	i_d (A)	i_q (A)	I_s (A)	t_s (s)	i_d (A)	i_q (A)	I_s (A)	t_s (s)
7	15	−2.6	8.85	9.22	0.1	−3.3	8.60	9.21	0.6	−3.0	8.73	9.20	0.7
4	7	−2.8	9.39	9.80	0.1	−0.7	9.70	9.73	1.1	−1.5	9.58	9.71	1.5
7	9	−3.0	9.50	9.95	0.1	−1.7	9.64	9.80	0.7	−1.1	9.71	9.77	1.1

In Table 3, we can find that when the d-axis inductance value and the q-axis inductance value increase or decrease at the same time, or one increases and the other decreases, the stator current value required by the IVSIC method (9.20 A, 9.71 A, 9.77 A) is the smallest. It can also be seen that although the IVSIC method increases efficiency compared to the VSIC method, the increased efficiency is less than that between the VSIC method and the FC method. Taking the third parameter change case as an example, the IVSIC method (9.77 A) reduces the stator current by 0.03 A compared to the VSIC method (9.80 A), and the VSIC method (9.80 A) reduces the stator current by 0.15 A compared to the FC method (9.95 A). This can also be explained by the side that the influence of the q-axis inductance parameters on the motor control efficiency is greater than that of the d-axis inductance parameters. At the same time, it can also be found that the mathematical relationship between the d-axis current value, the q-axis current value, and the stator current value satisfies Equation (3), which verifies the validity of the data. Additionally, when the parameter changes, the longest current transition time was obtained using the IVSIC method (0.7 s, 1.5 s, 1.1 s). It can be seen that the control speed drops when using the IVSIC method.

6. Conclusions

Aiming at the problem that the MTPA trajectory deviates due to changes in the motor parameters when the IPMSM is in MTPA control mode when using VSIC, in this paper, we proposed the online identification of the inductance by using MRAS and realize MTPA trajectory adjustment with changes in motor inductance parameters. The identifier model designed using this method is easy to implement, has strong practicability, and has a good parameter identification effect. The simulation results showed that the control strategy can inherit the performance of VSIC control well and has good robustness to changes in shaft inductance, thereby greatly improving the anti-interference ability of the system. However, this control method is relatively complex, and the application cost is high, so it is suitable for applications with relatively high-performance requirements.

Author Contributions: Conceptualization, N.-Z.J. and K.Z.; Methodology, N.-Z.J. and H.-C.C.; software, H.-C.C., Z.-Q.W. and L.Z.; validation, H.-C.C., Z.-Q.W. and L.Z.; supervision, N.-Z.J., K.Z. and D.-Y.S.; writing-original draft, H.-C.C.; writing-review and editing, N.-Z.J., H.-C.C. and D.-Y.S. All authors have read and agreed to the published version of the manuscript.

Funding: This research was funded by The Natural Science Foundation of Heilongjiang Province Joint Guide Project of China, grant number LH2021E086.

Conflicts of Interest: The authors declare no conflict of interest. The funders had no role in the design of the study; in the collection, analyses, or interpretation of data; in the writing of the manuscript, or in the decision to publish the results.

References

1. Zhu, J. Application present situation & development trend of rare earths permanent magnet motor. *Heavy Mach. Sci. Technol.* **2008**, *4*, 38–42.
2. Dutta, R.; Rahman, M.F. Design and analysis of an interior permanent magnet (IPM) machine with very wide constant power operation range. *IEEE Trans. Energy Convers.* **2008**, *23*, 25–33. [CrossRef]
3. Zhu, Z.Q.; Howe, D. Electrical machines and drives for electric, hybrid, and fuel cell vehicles. *Proc. IEEE* **2007**, *95*, 746. [CrossRef]
4. Li, C.H.; Chen, M.J. Study of a maximum ratio of torque to current control method for PMSM. *Proc. CSEE* **2005**, *25*, 169–174.

5. Kim, S.; Yoon, Y.D.; Sul, S.K. Parameter independent maximum torque per ampere (MTPA) control of IPM machine based on signal injection. In Proceedings of the IEEE Applied Power Electronics Conference and Exposition, Palm Springs, CA, USA, 21–25 February 2010.
6. Cheng, B.; Tesch, T.R. Torque feedforward control technique for permanent-magnet synchronous motors. *IEEE Trans. Ind. Electro.* **2010**, *57*, 969–974. [CrossRef]
7. Liao, Y.; Wu, Z.D.; Liu, R. Improved maximum torque per ampere control strategy study for PMSM used in electric vehicles. *Electr. Mach. Control* **2012**, *16*, 12–17.
8. Tang, Q.P.; Shen, A.W.; Luo, P. IPMSMs sensorless MTPA control based on virtual q-axis inductance by using virtual high-frequency signal injection. *IEEE Trans. Ind. Electron.* **2020**, *67*, 136–146. [CrossRef]
9. Liu, G.H.; Wang, J.; Zhao, W.X. A novel MTPA control strategy for IPMSM drives by space vector signal injection. *IEEE Trans. Ind. Electron.* **2017**, *64*, 9243–9252. [CrossRef]
10. Sun, T.F.; Wang, J.B.; Chen, X. Maximum Torque Per Ampere (MTPA) Control for Interior Permanent Magnet Synchronous Machine Drives Based on Virtual Signal Injection. *IEEE Trans. Power Electron.* **2015**, *30*, 5036–5045. [CrossRef]
11. Wang, J.; Huang, X.Y.; Yu, T. An Accurate Virtual Signal Injection Control of MTPA for an IPMSM with Fast Dynamic Response. *IEEE Trans. Power Electron.* **2018**, *33*, 7916–7926. [CrossRef]
12. Yang, Z.J.; Wang, L.N. Online multi-parameter identification for surface-mounted permanent magnet synchronous motors. *Trans. China Electrotech. Soc.* **2014**, *29*, 111–118.
13. Xun, Q.; Wang, P.L.; Li, Z.X. PMSM parameters identification based on recursive least square method. *Trans. China Electrotech. Soc.* **2016**, *31*, 161–169.
14. Wen, C.B.; Qi, L. On-line detection method of magnet flux linkage for permanent magnet synchronous motor. *Proc. CSU-EPSA* **2010**, *22*, 22–26.
15. Salvatore, N.; Caponio, A.; Neri, F. Optimization of delayed-state Kalman-filter-based algorithm via differential evolution for sensorless control of induction motors. *IEEE Trans. Ind. Electro.* **2010**, *57*, 385–394. [CrossRef]
16. An, Q.T.; Sun, L.; Zhao, K. An adaptive on-line identification method for the parameters of permanent magnet synchronous motor. *Trans. China Electrotech. Soc.* **2008**, *23*, 31–35.
17. Wang, L.H.; Zhang, X.; Zhang, W.F. Parameter identification of permanent magnet synchronous motor based on neural network. *Power Electron.* **2020**, *54*, 47–49.
18. Shi, W.G.; Yan, X.Y. Improved particle swarm algorithm of parameter identification for PMSM based on cloud model. *J. Dalian Jiaotong Univ.* **2019**, *40*, 113–119.
19. Zhong, W.P. Parameter Identification of Permanent Magnet Synchronous Motor Based on Genetic Algorithm. Master's Thesis, Changsha University of Science and Technology, Changsha, China, 2019.